HHS Public Access

Author manuscript

Sci Transl Med. Author manuscript; available in PMC 2019 September 03.

Published in final edited form as:

Sci Transl Med. 2017 February 01; 9(375): . doi:10.1126/scitranslmed.aah6510.

Tumor-homing cytotoxic human induced neural stem cells for cancer therapy

Juli R. Bagó[1], **Onyi Okolie**[1], **Raluca Dumitru**[2], **Matthew G. Ewend**[3,4], **Joel S. Parker**[4], **Ryan Vander Werff**[5], **T. Michael Underhill**[5], **Ralf S. Schmid**[6], **C. Ryan Miller**[4,6], **Shawn D. Hingtgen**[1,3,4,7,*]

[1]Division of Molecular Pharmaceutics, UNC Eshelman School of Pharmacy, University of North Carolina at Chapel Hill, Chapel Hill, NC 27599, USA.

[2]UNC Human Pluripotent Stem Cell Core Facility, Department of Genetics, UNC School of Medicine, University of North Carolina at Chapel Hill, Chapel Hill, NC 27599, USA.

[3]Department of Neurosurgery, UNC School of Medicine, University of North Carolina at Chapel Hill, Chapel Hill, NC 27599, USA.

[4]Lineberger Comprehensive Cancer Center, University of North Carolina at Chapel Hill, Chapel Hill, NC 27599, USA.

[5]Department of Cellular and Physiological Sciences, Biomedical Research Centre, University of British Columbia, Vancouver, British Columbia V6T 1Z3, Canada.

[6]Division of Neuropathology and Department of Pathology and Laboratory Medicine, Department of Neurology and Neuroscience Center, University of North Carolina at Chapel Hill, Chapel Hill, NC 27599, USA.

[7]Biomedical Research Imaging Center, University of North Carolina at Chapel Hill, Chapel Hill, NC 27599, USA.

Abstract

Engineered neural stem cells (NSCs) are a promising approach to treating glioblastoma (GBM). The ideal NSC drug carrier for clinical use should be easily isolated and autologous to avoid immune rejection. We transdifferentiated (TD) human fibroblasts into tumor-homing early-stage induced NSCs (h-iNSC^{TE}), engineered them to express optical reporters and different therapeutic gene products, and assessed the tumor-homing migration and therapeutic efficacy of cytotoxic h-

*Corresponding author: hingtgen@email.unc.edu.

Author contributions: J.R.B. designed and conducted all experiments. O.O. assisted with in vivo animal studies. R.D. assisted in experimental design, conducted aspects of h-iNSC^{TE} generation, and conducted RT-PCR and in vitro cell staining. M.G.E. contributed to the experimental design of multiple in vitro and in vivo studies. J.S.P. analyzed the RNA-seq results. R.S.S., R.V.W., and T.M.U. performed the RNA-seq. C.R.M. contributed to the design of multiple studies and assisted with the RNA-seq analysis. S.D.H. designed and supervised all experiments. S.D.H. and J.R.B. wrote the manuscript, with every author contributing comments.

SUPPLEMENTARY MATERIALS

www.sciencetranslationalmedicine.org/cgi/content/full/9/375/eaah6510/DC1

Data and materials availability: Materials are available to noncommercial researchers through a material transfer agreement with the UNC at Chapel Hill. The data for these studies have been deposited at the Gene Expression Omnibus (accession number GSE92839).

Competing interests: S.D.H., J.R.B., R.D., and M.G.E. are co-inventors on provisional patents filed with UNC at Chapel Hill related to aspects of human iNSC generation. S.D.H. and M.G.E. are founding members of Falcon Therapeutics. The other authors declare that they have no competing interests.

iNSC^{TE} in patient-derived GBM models of surgical and nonsurgical disease. Molecular and functional analysis revealed that our single-factor SOX2 TD strategy converted human skin fibroblasts into h-iNSC^{TE} that were nestin^{+} and expressed pathways associated with tumor-homing migration in 4 days. Time-lapse motion analysis showed that h-iNSC^{TE} rapidly migrated to human GBM cells and penetrated human GBM spheroids, a process inhibited by blockade of CXCR4. Serial imaging showed that h-iNSC^{TE} delivery of the proapoptotic agent tumor necrosis factor–a–related apoptosis-inducing ligand (TRAIL) reduced the size of solid human GBM xenografts 250-fold in 3 weeks and prolonged median survival from 22 to 49 days. Additionally, h-iNSC^{TE} thymidine kinase/ganciclovir enzyme/prodrug therapy (h-iNSC^{TE}–TK) reduced the size of patient-derived GBM xenografts 20-fold and extended survival from 32 to 62 days. Mimicking clinical NSC therapy, h-iNSC^{TE}–TK therapy delivered into the postoperative surgical resection cavity delayed the regrowth of residual GBMs threefold and prolonged survival from 46 to 60 days. These results suggest that TD of human skin into h-iNSC^{TE} is a platform for creating tumor-homing cytotoxic cell therapies for cancer, where the potential to avoid carrier rejection could maximize treatment durability in human trials.

INTRODUCTION

Cancers of the brain remain among the most challenging tumors to treat (1). More than 10,000 patients are diagnosed each year with glioblastoma (GBM), the most common primary brain tumor. GBM is treated with surgery and chemoradiation therapy, but the disease is universally fatal. Average time to recurrence is only 6 months, and average survival for GBM patients is 12 to 15 months. One of the most promising strategies to treat GBM is engineered neural stem cells (NSCs) (2). NSCs naturally migrate to solid and diffuse GBM deposits in response to chemotactic signals released by the cancer cells (3–6). When engineered with different cytotoxic agents, NSC therapy reduces GBM xenografts' volumes by 70 to 90% and extends the survival of tumor-bearing mice (2, 3, 7–10). On the strength of these preclinical studies, the first phase 1 trial of cytotoxic NSC therapy for GBM was recently completed (identifier:). Allogeneic NSCs that convert 5-fluorocytosine to 5-fluorouracil were delivered into the walls of the postsurgical resection cavity and found to be well tolerated in patients. Two additional phase 1 trials have now been launched to further develop this promising approach (identifiers: and). Although preclinical and clinical testing has relied heavily on allogeneic NSCs, autologous patient-derived NSC therapies could be highly advantageous in clinical use. The ability of autologous NSC therapy to avoid immune rejection not only would eliminate the complications of immunosuppressive regimens but also could prolong cytotoxic NSC persistence to increase both GBM killing and treatment durability. Unfortunately, isolation of autologous NSCs for GBM therapy remains a major challenge (11).

Reprogramming a patient's own somatic cells to create autologous cell therapies has opened therapeutic possibilities for cell-based central nervous system (CNS) treatment (12). Transdifferentiation (TD), in particular, is critically important for cell transplant therapies (13). TD directly converts fully differentiated somatic cells into somatic cells of a different type. This is accomplished without passing through an undifferentiated pluripotent state and increases the rate and efficiency of conversion as well as the in vivo safety (14–19). Thus,

TD cells are ideal for cell replacement, and they avoid immune surveillance because they are the patient's own cells (20). After the initial reports of TD in mouse cells (14–17), subsequent discoveries showed that TD can be used to create human NSCs, referred to as induced NSCs (h-iNSCs) (18, 19). This finding suggests that TD can be used to create patientspecific therapies for CNS disorders. However, the efficacy of TD-derived h-iNSC therapy for cancer has not been explored.

As an initial step toward developing an easily translatable personalized h-iNSC therapy for GBM, we provide evidence that TD-derived h-iNSC therapies can serve as tumor-homing drug carriers that inhibit the progression of GBM. Time is a priority for GBM patient therapy, and our TD strategy is capable of rapidly converting human skin fibroblasts into early-stage tumor-homing iNSCs (h-iNSC^{TE})in only 4 days, as confirmed by molecular and functional profiling of the cells. We then engineered h-iNSC^{TE} with optical reporters and cytotoxic agents and investigated the fate and tumor-specific homing of cytotoxic h-iNSC^{TE} using a combination of real-time molecular imaging, three-dimensional (3D) cell culture, and mouse models of human GBM. Next, we used therapeutic h-iNSC^{TE} engineered with the secreted proapoptotic protein tumor necrosis factor–α–related apoptosisinducing ligand (TRAIL) or enzyme/prodrug therapy and mouse models of both established orthotopic patient-derived tumor xenografts and diffuse postsurgical residual disease to investigate the efficacy of h-iNSC^{TE} therapy for GBM.

RESULTS

h-iNSC therapies for cancer

To create h-iNSC therapies for cancer treatment, we developed a TD strategy that is faster than previous reports to be compatible with the time frame for clinical GBM patient care (outlined in Fig. 1A) (18, 19). Normal human fibroblasts were transduced with SOX2 (SOX2/NHF) and cultured in NSC-inducing medium (Fig. 1B). Within 48 hours, the morphology of the SOX2/NHF changed, the cells formed neurospheres, and expression of the NSC marker nestin was detected and remained constant through day 10 (Fig. 1, B and C). Genetic engineering of the SOX2/NHF with lentivirus encoding green fluorescent protein (GFP) and firefly luciferase resulted in robust GFP expression. The cells retained high nestin expression and differentiated into GFAP^{+} astrocytes and TUJ-1^{+} neurons but lacked the pluripotency markers TRA-1–60 and OCT-4 (Fig. 1D). This was confirmed by real-time polymerase chain reaction (RT-PCR) analysis, which showed that the SOX2/NHF cells expressed the NSC marker nestin at levels ninefold higher than parental fibroblasts and threefold higher than human induced pluripotent stem cells (h-iPSCs) (Fig. 1E). SOX2 expression was high in both SOX2/NHF and h-iPSCs because SOX2 overexpression was used to generate both cell lines. Unlike h-iPSCs, SOX2/NHF did not have high expression of the pluripotency markers nanog or OCT-4. On the basis of these morphologic, genetic, and functional assays, we concluded that TD-converted SOX2/NHF were h-iNSCs.

A recent study revealed that a continuum of genetic changes occurs because fibroblasts are directly reprogrammed into iNSCs (21). We performed RNA sequencing (RNA-seq) to investigate the expression profile of h-iNSCs with a focus on key biologic parameters of tumor-homing cell migration. Differential expression analysis revealed substantial

transcriptional changes in h-iNSCs compared to the parental fibroblasts (Fig. 2, A and B), with 2810 genes up-regulated and 2660 genes down-regulated at day 5 after induction. Tumor-homing migration is one of the most critical aspects of stem cell therapy for cancer, unlike regenerative medicine. When we focused on genes that fall into the category of cell migration (22–24), we found that they were enhanced in both h-iNSCs and control brain-derived NSCs, suggesting that h-iNSCs have tumor-homing properties displayed by brain-derived NSCs (Fig. 2C). Additionally, genes associated with neuron development, ion transport, organ morphogenesis, and immune response were activated in both h-iNSC and NSC. Previously, similar pathway expression was reported in early-stage iNSCs because they transitioned from fibroblasts to mature iNSCs that closely resembled brain-derived NSCs (21). When we analyzed pathways related to tumor-homing migration, we found that *CXCR4*, *FLT1*, *HIF1A*, and *ANXA2* all showed changes in expression as fibroblasts converted to iNSCs (Fig. 2, D and E). Together, these results suggest that our rapid TD process generates early-stage iNSCs whose expression of tumor-homing pathways makes them suitable carriers for cancer treatment. To avoid confusion with previous studies, these cells will be referred to as h-iNSC^{TE}.

Assessing the tumor-homing properties of human iNSCs

Tumor-homing migration is one of the most distinctive and beneficial aspects of wild-type NSC therapy. Because expression analysis revealed that the pathways related to tumor-homing are increased in these cells, we next used real-time motion analysis to investigate the tumor-tropic nature of skin-derived h-iNSC^{TE}. h-iNSC^{TE}–mC-FL were seeded adjacent to GFP^{+} human GBM cells. Fluorescent timelapse images showed that h-iNSC^{TE} rapidly migrated toward the human GBM cells, with the leading edge covering the 500-mm gap in 22 hours (Fig. 3A and movie S1). Analyzing the migratory path of single cells confirmed the directional migration of h-iNSC^{TE} toward the GBM cells (Fig. 3C and movies S2 and S3). This tumor-directed migration was specific to the h-iNSC^{TE}, whereas the parental NHF exhibited nondirected random migration with minimal displacement toward the GBM cells (Fig. 3, B to D, and movies S4 to S6). h-iNSC^{TE} migrated in a more directed pattern, displaying a directionality index of 0.65 compared to NHF that displayed a more random migration index of 0.28 (Fig. 3D). h-iNSC^{TE} also migrated a longer Euclidean distance than NHF (340 μm versus 200 μm) (Fig. 3E). Last, we mimicked the in vivo migration of h-iNSC^{TE} into established GBM foci using 3D cell spheroid cultures. h-iNSC^{TE}–mC-FL spheroids were cocultured with GFP^{+} GBM spheroids, and both cell types were levitated using magnetic force. h-iNSC^{TE} were found to penetrate the GBM spheroids within hours of seeding (Fig. 3F) and continued migrating into the core of the GBM spheroid through 7 days of culture. CXCR4 is one of the most wellestablished mediators of tumoritropic homing (22, 24). RT-PCR analysis confirmed that CXCR4 expression was increased 4.3-fold after fibroblasts were converted into h-iNSC^{TE} (Fig. 3G). Further, pretreatment of h-iNSC^{TE} with CXCR4-blocking antibodies markedly reduced the tumor-homing capacity of the cells compared to untreated cells in our coculture migration assays (Fig. 3, H to J, and movies S7 and S8). Together, these observations support the conclusion that h-iNSC^{TE} have tumoritropic properties that allow them to migrate to GBM cells.

h-iNSC^{TE} therapy of human GBM xenografts in mice

To monitor h-iNSC^{TE} in vivo, we engineered the cells to express the optical reporters mCherry and firefly luciferase (h-iNSC^{TE}–mC-FL). We found that the genetic engineering had minimal effect on proliferation because h-iNSC^{TE} and h-iNSC^{TE}–mC-FL grew at similar rates (Fig. 4A). To study the persistence of h-iNSC^{TE} in the brain, we stereotactically implanted h-iNSC^{TE}–mC-FL into the brains of mice. Real-time noninvasive imaging showed that h-iNSC^{TE} persisted through 21 days but were gradually cleared (Fig. 4B). Revealing the fate of the h-iNSC^{TE}, postmortem immunohistochemistry showed that numerous h-iNSC^{TE}–mC-FL expressed the NSC marker nestin (Fig. 4C). A portion of h-iNSC^{TE} stained positive for the neuronal marker TUJ-1 (Fig. 4C), but minimal staining was detected for the astrocyte marker GFAP (Fig. 4C). No OCT-4 and TRA-1–60 expression was detected, indicating that the transplanted h-iNSC^{TE} do not express markers of a potentially carcinogenic pluripotent intermediate in vivo. Together, these findings suggest that the h-iNSC^{TE} survive in the murine brain, do not exhibit malignant transformation, and express markers of NSCs as well as potentially differentiate into cells of a neural lineage.

We first tested the efficacy of h-iNSC^{TE} delivery of a secreted cytotoxic agent for the treatment of solid GBM. h-iNSC^{TE} were engineered to express a secreted variant of the proapoptotic molecule TRAIL (h-iNSC^{TE}–sTR; Fig. 5, A and B). The anti-GBM effects of TRAIL are well established, and the agent has been extensively used in cell-based GBM therapy (3, 8, 25, 26). h-iNSC^{TE}–sTR or control iNSC–GFP-RL were mixed at different ratios with mC-FL^{+} human GBM cells in 3D culture for 48 hours. Fluorescence imaging and bioluminescence imaging (BLI) of GBM cell volumes showed that h-iNSC^{TE}–sTR markedly reduced the viability of 3D GBM spheroids compared to control-treated tumors in a dose-dependent pattern (Fig. 5C).

To test the efficacy of h-iNSC^{TE}–sTR–based therapy against solid GBM in vivo, we implanted human U87 GBM cells expressing mC-FL with h-iNSC^{TE}–sTR or control h-iNSC^{TE}–GFP (Fig. 5D) into the brain parenchyma of mice. Serial BLI of tumor volumes showed that h-iNSC^{TE}–sTR treatment inhibited tumor growth by day 3, resulting in GBM volumes that were 50-fold smaller than in control animals by day 24 (Fig. 5, E and F). Survival analysis showed that h-iNSC^{TE}–sTR– treated animals survived an average of 51 days, whereas control animal succumbed to GBM in only 25 days (Fig. 5G). Postmortem analysis showed the h-iNSC^{TE}–sTR staining positive for TRAIL 2 weeks after implantation. Additionally, the h-iNSC^{TE}–sTR in the GBM stained positive for nestin and TUJ-1 but were negative for GFAP and pluripotency markers OCT-4 and TRA-1–60 (Fig. 5H). These data show that h-iNSC^{TE} delivery of a secreted cytotoxic agent inhibits the growth of solid GBM and prolongs the survival of tumor-bearing animals.

We next explored the efficacy of h-iNSC^{TE} prodrug/enzyme therapy against human patient–derived GBMs that more accurately mimics the clinical treatment of the disease (9). We engineered h-iNSC^{TE} with a bifunctional reporter including red fluorescent protein (RFP) and thymidine kinase (h-iNSC^{TE}–TK). Cell viability assays showed that mixing (Fig. 6, A, B, and E) or side-by-side culturing (Fig. 6, C to E) of h-iNSC^{TE}–TK with GBM4 patient–derived CD133^{+} human GBM–initiating cells expressing GFP and FL (GBM4–GFP-FL) markedly reduced tumorspheroid viability compared to control-treated tumor spheroids after

the addition of the ganciclovir (GCV) prodrug. h-iNSC^{TE}–TK^{+}GCV killing of the established GBM spheroids was slower than in cell mixtures, likely because the therapeutic cells were not evenly distributed throughout the tumor spheroid as in the mixed model (Fig. 6E).

We next determined the efficacy of h-iNSC^{TE}–TK therapy against established GBM4 in vivo. GBM4–GFP-FL cells were implanted into the brain parenchyma of mice. Three days later, h-iNSC^{TE}–TK were injected into the established tumors, and GCV or saline was administered to the animals (Fig. 6F). Serial BLI showed that h-iNSC^{TE}–TK^{+}GCV–treated tumors were 20-fold smaller than control 28 days after injection (Fig. 6G). The treatment significantly ($P = 0.0018$) extended the median survival of tumor-bearing mice (GCV, 67 days; control, 37 days; Fig. 6H). Fluorescent imaging of postmortem tissue sections verified the reduction in tumor volumes by h-iNSC^{TE}–TK therapy (Fig. 6, I and J). Large tumors were present in the brains of control-treated animals, yet only a few residual cells were detected in h-iNSC^{TE}–TK^{+}GCV–treated mice. Together, these results show that h-iNSC^{TE}–TK prodrug/enzyme therapy has therapeutic effects against patient-derived GBM and markedly prolongs the survival of tumor-bearing mice.

Intracavity h-iNSC^{TE} prodrug/enzyme treatment of postsurgical minimal patient-derived GBM in mice

Surgical resection is part of the clinical standard of care for GBM patients (1). We next used our mouse models of GBM resection/recurrence and synthetic extracellular matrix encapsulation (sECM) strategies to determine the efficacy of h-iNSC^{TE}–TK therapy for surgically resected GBMs (26, 27). To investigate the migration of h-iNSC^{TE}–TK encapsulated in sECM, we performed 3D cultures of the encapsulated h-iNSC^{TE} with GFP-FL^{+} GBM8 spheroids (patient-derived CD133^{+} human GBM–initiating cells; Fig. 7A). We found that mCherry^{+} h-iNSC^{TE} migrated from the sECM and populated GFP^{+} GBM8 spheroids within 3 days (Fig. 7B). 3D coculture assays showed that sECM/h-iNSC^{TE}–TK therapy markedly reduced the viability of GBM8 spheroids after addition of GCV (Fig. 7C).

To mimic h-iNSC^{TE} therapy for human patients with surgically resected GBM, invasive patient-derived GBM8 cells were implanted into the brain parenchyma of mice (Fig. 7D). Ten days later, the established tumors were surgically resected. h-iNSC^{TE}–TK were encapsulated in sECM and transplanted into the surgical resection cavity, and mice were treated with GCV or saline. Serial BLI showed that h-iNSC^{TE}–TK^{+}GCV therapy attenuated the regrowth of GBM8 tumors such that residual tumors were 3.5-fold smaller in the treated animals compared to control 14 days after h-iNSC^{TE}–TK implantation (Fig. 7E). h-iNSC^{TE}–TK^{+}GCV therapy also extended median survival, with h-iNSC^{TE}–TK^{+}GCV–treated animals surviving an average of 60 days compared to 46 days in control-treated mice (Fig. 7F).

DISCUSSION

Cytotoxic NSC therapy for GBM recently entered phase 1 clinical patient testing on the strength of preclinical studies (9). Here, we provide evidence that human fibroblast–derived h-iNSC^{TE} are tumor-homing drug carriers. Using clinically relevant mouse models and therapeutic agents, we show that h-iNSC^{TE} therapy regressed solid GBM and suppressed

recurrence of postsurgical GBM. These results position h-iNSC^{TE} technology as a feasible approach to eventual routine autologous therapy without the need for invasive brain biopsy or lifelong immunosuppressive treatment.

We sought to use next-generation cellular reprogramming to generate easily isolated and autologous NSC therapies for cancer therapy. In the clinical setting, the potential of autologous carriers, such as h-iNSC^{TE}, to avoid immune rejection could provide therapeutic advantages over allogeneic NSC therapies currently used in clinical trials. Studies using reprogramming technology for cancer therapy are limited; however, initial studies harnessed iPSC technology to establish proof of concept. Yamazoe *et al.* showed that mouse NSCs derived by the multistage iPSC process have the capacity to home to GBM both in vitro and in vivo (28). Yang *et al.* used human iPSC-NSC and showed that the tumorhoming migration of these cells is not limited to the brain because they could seek out metastatic breast cancer foci when infused intravenously (29). Zhu *et al.* extended these findings into therapy, showing that iPSC-NSC delivery of prodrug/enzyme therapy slowed progression of metastatic breast cancer xenografts, and both killing and safety were improved by additional modification with the vesicular stomatitis virus glycoprotein (30). Our approach uses cells created by TD, where fibroblasts are directly converted into iNSCs. The rapid generation of cells in this single-step process is essential for GBM treatment because patients have only months to live (31). Further, elimination of the potentially tumorigenic iPSC and embryoid body stages should help ensure that h-iNSC^{TE}/iNSCs are non–tumor-forming in vivo. The current study explores iNSC derived from human fibroblasts for cancer therapy. To further maximize the translational relevancy of our study, we used a SOX2 TD strategy that both eliminated the need for feeder cells and increased the rate of h-iNSC^{TE} generation compared to established TD methods (19). In vitro, forced differentiation produced h-iNSC^{TE} that differentiated into both astrocytes and neurons and did not express pluripotency markers. In vivo, the h-iNSC^{TE} survived through 3 weeks and remained positive for nestin or TUJ-1 but did not express OCT-4 or TRA-1–60. The h-iNSC^{TE} were also potent drug delivery vehicles, rapidly migrating to GBM cells or spheroids and delivering cytotoxic gene products to reduce GBM progression.

We found that h-iNSC^{TE} share key similarities with traditional brain-derived NSCs used for cancer therapy (4, 6, 9, 32, 33). For studies focusing on the use of NSC/iNSCs for cancer treatment, the ability of the cells to seek out cancer foci and deliver cytotoxic agents is essential (2, 34). Although the focus of our study was on the development of iNSCs for cancer therapy rather than regenerative medicine, we found that h-iNSC^{TE} had high expression of nestin and differentiated into appropriate neural lineages in vitro and in vivo, a key attribute of brain-derived NSCs. Our genetic analysis revealed numerous similarities in the expression profiles of the two cell types. Critical for use as drug carriers, h-iNSC^{TE} showed high expression of pathways implicated in mediating the tumor-homing capacity of wild-type NSCs. In particular, RT-PCR analysis showed that CXCR4, the most well-established mediator of tumor homing in brain-derived NSCs (22, 24), was markedly up-regulated as fibroblasts were converted into h-iNSC^{TE}. Functional studies showed that h-iNSC^{TE} rapidly migrated to human GBM cells and penetrated into GBM spheroids. We and others previously reported the ability of human brain–derived NSCs to migrate to GBM, where they also penetrated the borders of the established tumor (3–5). Functional assays also

identified CXCR4 as a key mediator of h-iNSC^{TE} tumoritropic homing, in agreement with studies demonstrating a central role for this receptor in the tumor-homing migration of brain-derived NSC drug carriers (24). Exploring further similarities to brain-derived NSC therapies, we found that the h-iNSC^{TE} were gradually cleared over 14 days in vivo, with most of the cells having cleared by day 25. This persistence was very similar to our previous findings using human brain–derived NSCs delivered in the context of GBM (4). Additionally, both h-iNSC^{TE} and wild-type NSCs remained predominantly nestin^{+} after implantation. We believe that these data validate h-iNSC^{TE} as tumor-homing drug carriers for use as anticancer therapies. The rapid generation of h-iNSC^{TE} should enable scale-up and generation of clinical numbers of therapeutic cells within the small therapeutic window required for patient trials. Further studies will be required to determine the ability of h-iNSC^{TE} to seek out other solid cancer types, as well as the potential to accumulate selectively in tumors after intravenous infusion.

We used h-iNSC^{TE} engineered with two different cytotoxic agents. TRAIL is a secreted proapoptotic agent that has been used extensively in preclinical NSC-based GBM therapy (3, 8, 35, 36). We found that h-iNSC^{TE}–sTR treatment reduced the viability of U87 GBM spheroids in 3D cultures and markedly reduced tumor volumes in vivo. Clinical NSC therapy for GBM uses a prodrug/enzyme approach (9). Therefore, we also used h-iNSC^{TE}–TK^{+}GCV therapy. In this approach, nontoxic GCV is phosphorylated by TK in the h-iNSC^{TE} and converted to a toxic compound that diffuses into neighboring tumor cells to induce death (37). Our data showed that h-iNSC^{TE}–TK could kill solid patient-derived GBM4 spheroids. The killing was slower than when h-iNSC^{TE}–TK were mixed throughout the GBM spheroid but closely matched the in vivo killing kinetics when h-iNSC^{TE}–TK were injected into established GBM4 tumors in the brains of mice. These data demonstrate that h-iNSC^{TE} prodrug/enzyme therapy is a feasible approach to reduce GBM volumes. The current standard of care for GBM consists of surgery, temozolomide (TMZ), and radiation. This approach was adopted in 2005 after the publication of the landmark phase 3 trial showing that inclusion of TMZ with fractionated radiation and surgery extended median survival of newly diagnosed GBM patients from 12.1 to 14.6 months (38). Numerous preclinical studies have investigated the impact of each clinical treatment independently. Many of these studies used established cell lines, allowing for direct comparison to the U87 used in our study. In previous studies investigating the impact of radiation on U87 growth, it was reported that 8 Gy extends survival of U87-bearing mice from about 29 to 38 days (39). Investigating TMZ, a meta-analysis of more than 2443 mice showed an average increase in median survival of 1.88-fold and average reduction in tumor volumes of 50% (40, 41). Data specifically on U87 were similar, showing reductions in tumor volume of just greater than 50% and increased survival around 1.7-fold. Data on the impact of surgical resection are limited by the lack of preclinical models incorporating resection. We previously found that surgical debulking of U87 intracranial xenografts extended the survival from 25 to 32 days (26). Here, we found that h-iNSC^{TE} therapy reduced U87 tumor volumes 250-fold at 3 weeks after treatment and increased survival 2.23-fold. When compared to these reported preclinical studies using the clinical standard of care, our findings suggest that h-iNSC^{TE} therapy could be an effective treatment option to improve care for GBM patients.

Surgical resection is part of the clinical standard of care for GBM patients (1). Yet, solid GBM xenografts have been the standard model used to characterize GBM therapies (2). In our study, 3D culture systems show that both h-iNSC^{TE}–TK spheroids and sECM-encapsulated h-iNSC^{TE}–TK killed patient-derived GBM spheroids in a time frame that closely mirrored the in vivo tumor response. Our results showed that h-iNSC^{TE}–sTR treatment regressed solid U87 GBM xenografts in vivo and prolonged the survival of tumor-bearing mice. h-iNSC^{TE}–TK treatment had similar effects against established patient-derived GBM4 xenografts. Using our image-guided model of GBM resection/recurrence in mice (27), we found that intracavity h-iNSC^{TE}–TK treatment suppressed the regrowth of patient-derived GBM8 xenografts. Extensions in survival were not as pronounced in solid GBM treatment. The exact reason is unknown but could be due to the challenge of eradicating the highly invasive GBM8 tumor cells (42). Yet, our results demonstrate that cytotoxic h-iNSC^{TE} treatment can inhibit the progression of solid tumors and recurrence of postsurgical patient-derived GBM xenografts.

NSC therapy for GBM is rapidly expanding in the clinic (9, 33). h-iNSC^{TE} therapy could address the challenge of personalized NSC drug carriers that potentially limit allogeneic treatments currently under clinical testing. The effectiveness of stem cell–based cancer therapies is reliant on their ability to seek out distant cancer foci and function as in vivo drug pumps to deliver cytotoxic agents for extended durations. The prospects of personalized drug carriers, such as h-iNSC^{TE}, to avoid immune rejection in patients suggest the potential for longer persistence in human patients compared to allogeneic therapies. This would, in turn, create a larger window during which the therapeutic cells could migrate, affording h-iNSC^{TE} the increased time required to track down invasive tumor spread at long distances from the resection cavity. This will be particularly important in clinical testing, where therapeutic cells will be required to track down invasive GBM foci on the scale of the human brain. The longer persistence should also prolong the duration of drug delivery, thus improving tumor kill and sustaining durable tumor suppression better than drug carriers that are rapidly cleared from the brain. Although data are limited, a previous study suggests that autologous cell implants generated by reprogramming do persist longer than allogeneic implants (43). Greater numbers of self-derived iPSC neurons were found to persist after transplant, cause only minor immune activation, and improve therapy compared to allogeneic transplant that resulted in activation of both microglia and leukocytes (43). Because our data support the conclusion that h-iNSC^{TE} are tumor-homing cell carriers with anticancer efficacy, this sets the stage for future studies comparing the precise benefits of this approach over traditional allogeneic cell carriers as well as other delivery systems including nanoparticles, oncolytic viruses, and chemotherapeutic agents.

In conclusion, these studies provide evidence that cytotoxic h-iNSC^{TE} are tumor-homing drug carriers that inhibit GBM progression in mouse models, which reflect the clinical scenario of GBM therapy. These findings should serve as a guide to design clinical trials where a patient’s own skin cells could be used to create cytotoxic drug carriers that are reimplanted into the patient to maximize tumor killing. This could have broad clinical impact, as cytotoxic NSC therapy is being explored for the treatment of metastatic (44), pediatric (45, 46), and peripheral cancer (47). The establishment of Good Manufacturing Practice facilities at numerous institutions and the entrance of reprogrammed cells into

human clinical trials support the feasibility of translating h-iNSC^{TE} and related therapies into the clinical setting.

MATERIALS AND METHODS

Study design

This preclinical study was designed to explore the efficacy of h-iNSC^{TE} as an approach to cancer therapy. We theorized that TD could be used to convert human skin fibroblasts into tumor-homing terapeutic iNSCs that could migrate to GBM cells and deliver therapeutic transgenes to inhibit pogression of the disease. We used multiple approaches to characterize the fate of tumoricidal h-iNSC^{TE}, their tumor-homing capacity, and their anti-GBM properties. These approaches included assaying cell migration using real-time kinetic tracking of in vitro coculture assays as well as 3D cell culture models. Tumor killing was determined with therapeutic h-iNSC^{TE} engineered with two different cytotoxic agents (TRAIL and TK/GCV) and tested in two different mouse models of GBM, where one model used orthotopic established GBMs and the other incorporated surgical tumor resection of patient-derived cancer lines. Animal numbers for each study are detailed in the relevant sections below. GBM volumes were determined using serial BLI. Mice were randomized into control and treatment groups based on the pretreatment BLI signal. Animals were monitored daily and euthanized at the onset of symptoms of debilitating disease, including weight loss, hunched posture, or impaired gait. We have included additional details on statistical analysis below.

Cell lines

U87 and 293T were purchased from the American Type Culture Collection. GBM8 and GBM4 were gifts from H. Wakimoto (Massachusetts General Hospital). Human fibroblasts were provided by W. Kauffman [University of North Carolina (UNC) School of Medicine]. All cells were grown as previously described (3, 42). Lentiviral vectors (LVs) encoding hTERT and SOX2 were purchased from Addgene. All complementary DNAs (cDNAs) were under the control of the tetracycline promoter.

Lentiviral vectors

In addition to the reprogramming vectors, the following LVs were used in this study: GFP fused to firefly luciferase (LV–GFP-FL), GFP fused to *Renilla* luciferase (LV–GFP-RL), mCherry protein fused to firefly luciferase (LV–mC-FL), a secreted variant of TRAIL (LV-sTR), and an RFP thymidine kinase fusion (LV-TK; Life Technologies). GFP-RL and GFP-FL were constructed by amplifying the cDNA encoding *Renilla* luciferase or firefly luciferase using the vectors luciferase-pcDNA3 and pAC-hRluc (Addgene), respectively. The restriction sites were incorporated in the primers, and the resulting fragment was digested with Bgl II and Sal I and ligated in-frame in Bgl II/Sal I–digested pEGFPC1 (Clontech). The GFP-FL or GFP-RL fragments were digested with Age I (blunted) and Sal I and ligated into pTK402-digested (provided by T. Kafri, UNC Gene Therapy Center) Bam HI (blunted) and Xho I to create LV–GFP-FL or LV–GFP-RL. Similarly, mC-FL was created by amplifying the cDNA encoding firefly luciferase from luciferase-pcDNA3, ligating into Bgl II/Sal I–digested mCherry-C1 (Clontech), and ligating the mC-FL fragment

into pTK402 LV backbone using blunt/Xho I sites. To create LV-sTR, the cDNA sequence encoding sTR was PCR-amplified using custom-synthesized oligonucleotide templates (Invitrogen). The restriction sites were incorporated into the primers, and the resulting fragment was digested with Bam HI and Xho I and ligated in-frame into Bam HI/Xho I–digested pLVX plasmid (a gift from S. Magness, UNC Department of Medicine). LV-sTR has IRES-GFP elements in the backbone as well as a cytomegalovirus-driven puromycin element. The bi-function TK virus was synthesized and cloned into the LV backbone by Life Technologies. All LV constructs were packaged as LV vectors in 293T cells using a helper virus–free packaging system as described previously (48). h-iNSC^{TE} and GBM cells were transduced with LVs at varying multiplicity of infection by incubating virions in a culture medium containing protamine sulfate (5 μg/ml; Sigma), and cells were visualized for fluorescent protein expression by fluorescence microscopy.

h-iNSC^{TE} generation

Human fibroblasts (200,000) were seeded in six-well plates and transduced with the LV cocktail containing hTERT and SOX2 in a medium containing protamine sulfate (5 μg/ml; Sigma). Two days after infection, the medium was changed to STEMdiff Neural Induction Medium (StemCell Technologies) containing doxycycline (10 μg/ml; Sigma). Medium was changed every 3 days. Neurosphere formation was induced by culturing in low-adherence flasks.

Cell viability and passage number

To assess the proliferation of modified and unmodified h-iNSC^{TE} and h-iNSC^{TE} expressing GFP-FL or sTR, the cells were seeded in 96-well plates. Cell viability was assessed 2 to 10 days after seeding using CellTiter-Glo luminescent cell viability kit (Promega).

Immunohistochemistry and in vitro differentiation

To determine the effects of LV modification on h-iNSC^{TE} differentiation, h-iNSC^{TE} were transduced with LV–GFP-FL or LV-sTR. Engineered or unmodified cells (1×10^5 cells per well) were seeded on coverslips, fixed, permeabilized, and incubated for 1 hour with anti-nestin polyclonal antibody (1:500; Millipore, ABD69). Cells were washed and incubated with the red secondary antibody (Biotium, 20038) for 1 hour. Cells were then washed, mounted, and imaged using fluorescence confocal microscopy. For differentiation, engineered or nontransduced h-iNSC^{TE} (1×10^5 cells per well) were cultured for 12 days in stem cell medium depleted of doxycycline, epidermal growth factor, and fibroblast growth factor. Cells were then stained with antibodies directed against nestin, GFAP (1:250; Millipore, MAB3402), or TUJ-1 (1:1000; Sigma, T8578) and detected with a red secondary antibody (Biotium). Nuclei were counterstained with Hoechst 33342, and the results were analyzed using an FV 1200 laser confocal microscope (Olympus).

RNA-seq analyses

Total RNA was extracted from human fibroblast, h-iNSC^{TE}, or brain-derived NSC cellular pellets using Qiagen RNeasy kits, followed by library preparation using a Stranded mRNA-seq kit (Kapa Biosystems) according to the manufacturer's instructions. High-throughput

sequencing with 43–base pair paired-end reads was performed on NextSeq 500 using the Illumina High Output kit and analyzed as previously described (49, 50). QC-passed reads passing Illumina's Purity Filter were aligned to the human reference genome (hg38) using MapSplice (51). The alignment profile was determined by Picard Tools v1.64 (http://broadinstitute.github.io/ picard/). Aligned reads were sorted and indexed using SAMtools, translated to transcriptome coordinates, and then filtered for indels, large inserts, and zero mapping quality using UBU v1.0 (https://github.com/ mozack/ubu). Transcript abundance estimates for each sample were calculated using RSEM, an expectation-maximization algorithm (52) using the University of California Santa Cruz known gene transcript and gene definitions. Before visualization, raw RSEM read counts for all RNA-seq samples were normalized to the overall upper quartile (53). PCA, cluster analysis, differential expression testing with DESeq2 (54), and plotting of these results were performed in R 3.2.1.

h-iNSC^{TE} survival and fate in vivo

To determine the survival of h-iNSC^{TE} in vivo, h-iNSC^{TE} expressing mC-FL (7.5×10^5 cells per mouse) were suspended in phosphatebuffered saline (PBS) and implanted stereotactically into the right frontal lobe of mice ($n = 7$). h-iNSC^{TE} survival was determined by serial BLI performed for 20 days using the IVIS In Vivo Imaging System. To determine the fate of h-iNSC^{TE} at a cellular resolution, animals were sacrificed 14 to 21 days after implantation, and their brains were extracted and sectioned. Tissue sections were stained with antibodies against nestin, GFAP, TUJ-1, OCT-4, and TRA-1–60 and visualized using a secondary antibody labeled with CF 488.

Real-time PCR

To assess the expression of *NESTIN*, *SOX2*, *NANOG*, *OCT-4*, and *CXCR4*, RT-PCR analysis was performed at the UNC Animal Clinical Chemistry and Gene Expression core facility using validated primer/probe sets for each target gene. Analysis was performed on an ABI 7300/7500 system. Data are expressed relative to *GAPDH* controls.

In vivo BLI

To track h-iNSC^{TE} fate or tumor progression, serial BLI was performed as described (55, 56). Briefly, mice were given an intraperitoneal injection of D-luciferin (4.5 mg per mouse in 150 μl of saline), and photon emission was assessed 5 min later using the IVIS Kinetic Optical System (PerkinElmer) with a 5-min acquisition time. Images were processed, and photon emission was quantified using the Living Image software (PerkinElmer). Additionally, mice were followed for survival over time.

3D tissue culture

3D levitation cell cultures were performed using the Bio-Assembler Kit (Nano3D Biosciences). Confluent six-well plates containing GBM or h-iNSC^{TE} (5×10^5 cells per well) were treated with a magnetic nanoparticle assembly [NanoShuttle (NS), Nano3D Biosciences] overnight according to the manufacturer's specifications. NS is a mixture of iron oxide and gold nanoparticles cross-linked with poly-L-lysine to promote cellular attachment. NS-treated GBM and h-iNSC^{TE} were then detached with trypsin, resuspended,

and mixed at different ratios (0.5:1 and 1:1) in an ultralow attachment six-well plate in 2 ml of medium. A plastic lid containing six magnetic drivers (neodymium magnet with field strength of 50 G) was placed on top of the plate to levitate the cells to the air-liquid interface. Cells were levitated for 24 hours to create cell spheroids.

3D coculture viability assays

3D levitation culture was used in three separate in vitro cytotoxicity studies. h-iNSC^{TE} expressing two different cytotoxic agents were used to treat one established GBM cell line (U87) and two patient-derived GBM lines (GBM4 and GBM8). To determine the cytotoxicity of TRAIL therapy, h-iNSC^{TE}–sTR or h-iNSC^{TE}–GFP spheroids were cocultured in suspension with U87–mC-FL spheroids at a ratio of 0.5:1 or 1:1 (iNSC/GBM). GBM spheroid viability was determined 48 hours later by FL imaging. To determine the cytotoxicity of prodrug enzyme therapy for patient-derived GBM4s, h-iNSC^{TE}–TK spheroids were cocultured in suspension with patient-derived GBM4–GFP-FL spheroids or mixed with GBM cells before sphere formation. Spheroids were cultured with or without GCV (UNC hospitals), and GBM spheroid viability was determined 0, 2, 4, or 7 days after addition of the prodrug by FL imaging. To determine the cytotoxicity of the sECM-encapsulated h-iNSC^{TE} prodrug/enzyme therapy, h-iNSC^{TE}–TK were encapsulated in sECM and placed in levitation culture with patient-derived GBM8–GFPFL spheroids. Viability was determined by FL imaging.

Real-time imaging and motion analysis

h-iNSC^{TE} migration was assessed in 2D and 3D culture systems. To assess 2D migration, h-iNSC^{TE} expressing LV–mC-FL were seeded in microculture inserts in glass bottom microwell dishes (MatTek) using two-chamber cell culture inserts (Ibidi). U87 glioma cells expressing GFP were plated into the adjacent well (0.5-mm separation). Twenty-four hours after plating, cells were placed in a Viva View live-cell imaging system (Olympus) and allowed to equilibrate. The insert was removed, and cells were imaged at ×10 magnification every 20 min for 22 hours in six locations per well in three independent experiments. NIH Image with chemotaxis and manual tracking plug-ins was used to generate movies and determine both the total distance migrated and the directionality of migration. To perform the CXCR4-blocking study, h-iNSC^{TE} were pretreated with anti-human CXCR4 monoclonal antibody (10 μg/ml; clone 12G5, R&D Systems) for 3 hours as described previously (57). 2D migration was then assessed as described above. For 3D migration, h-iNSC^{TE} migration to GBM spheroids was assessed in 3D culture systems by creating h-iNSC^{TE} and GBM spheroids using levitation culture as described above. h-iNSC^{TE} (red) and GBM (green) spheroids were cocultured in levitation systems. Real-time imaging was performed to visualize the penetration of GBM spheroids by h-iNSC^{TE} in suspension.

Anti-GBM efficacy of h-iNSC^{TE} therapy in vivo

Three different xenograft studies were performed to assess the anti-GBM effects of h-iNSC^{TE} engineered with two different cytotoxic agents. (i) To assess h-iNSC^{TE} therapy in solid GBM, h-iNSC^{TE}–sTR or iNSC–GFP-RL (5×10^5 cells per mouse) were stereotactically implanted into the right frontal lobe of mice ($n = 7$) together with U87–mC-FL cells (5×10^5 cells per mouse). Therapeutic response was then determined by monitoring

tumor volumes with FL BLI. (ii) To assess h-iNSC^{TE} prodrug/enzyme therapy for established patient-derived GBM, GBM4 cells expressing mC-FL (5×10^5 cells per mouse) were stereotactically implanted in the right frontal lobe of mice. Three days later, h-iNSC^{TE}–TK ($n = 7$, 5×10^5 cells per mouse) or h-iNSC^{TE}–mRFP-hRL ($n = 7$, 7.5×10^5 cells per mouse) were implanted into the established tumors. GCV was injected intraperitoneally daily for 2 weeks at a dose of 100 mg/kg. FL imaging was used to assess changes in tumor volume as described above, and mice were monitored for survival over time. (iii) To assess h-iNSC^{TE} therapy in surgically resected GBM, patient-derived GBM8–GFP-FL were harvested at 80% confluency and implanted stereotactically (5×10^5 cells) in the right frontal lobe: 2 mm lateral to the bregma and 0.5 mm from the dura. Ten days later, mice were immobilized on a stereotactic frame and placed under an Olympus MVX10 microscope. Intraoperative microscopic white light, GFP, and RFP images were captured throughout the procedure using a Hamamatsu ORCA 03G charge-coupled device camera and software (Olympus). A midline incision was made in the skin above the skull, exposing the cranium of the mouse. The intracranial xenograft was identified using GFP fluorescence. A small portion of the skull covering the tumor was surgically removed using a bone drill and forceps, and the overlying dura was gently peeled back from the cortical surface to expose the tumor. Under GFP fluorescence, the GBM8–GFP-FL tumor was surgically excised using a combination of surgical dissection and aspiration, and images of GFP were continuously captured to assess accuracy of GFP-guided surgical resection. h-iNSC^{TE}–TK or h-iNSC^{TE}–mC-FL (5×10^5 cells) were encapsulated in hyaluronic sECM hydrogels (Sigma) and transplanted into the postoperative GBM cavity, and skin was closed using surgical glue. Mice were then administered GCV as described above. No procedure-related mortality was observed. GBM recurrence was visualized by FL imaging as described above, and mice were followed for survival.

Tissue processing

Immediately after the last imaging session, mice were sacrificed and perfused with formalin, and their brains were extracted. The tissue was immediately immersed in formalin. Coronal sections (30 μm) were generated using a vibrating microtome (Fisher). For nestin, GFAP, and TUJ-1 staining, sections were incubated for 1 hour in a blocking solution (0.3% bovine serum albumin, 8% goat serum, and 0.3% Triton X-100) at room temperature, followed by incubation at 4°C overnight with the following primary antibodies diluted in blocking solution: (i) anti-human nestin (Millipore), (ii) anti-GFAP (Millipore), (iii) anti-TRAIL (Prosci), and (iv) anti–TUJ-1 (Sigma). Sections were washed three times with PBS, incubated in the appropriate secondary antibody, and visualized using a confocal microscope (Olympus).

Study approval

All experimental protocols were approved by the Animal Care and Use Committees at the UNC at Chapel Hill, and care of the mice was in accordance with the standards set forth by the National Institutes of Health *Guide for the Care and Use of Laboratory Animals*, U.S. Department of Agriculture regulations, and the American Veterinary Medical Association.

Statistical analysis

Data were analyzed by Student's t test and paired t test when comparing two groups, and by one- and two-way ANOVA and repeated measures when comparing more than two groups. Data were expressed as means ± SEM, and differences were considered significant at $P < 0.05$. Survival times of mouse groups were compared using log-rank test.

Supplementary Material

Refer to Web version on PubMed Central for supplementary material.

Acknowledgments:

We thank S. Henning and D. Ransohoff for insightful discussions, H. Wakimoto (Massachusetts General Hospital) for providing the GBM4 and GBM8 cell lines, W. Kauffman (UNC School of Medicine) for providing human fibroblast cell lines, and T. Kafri (UNC Gene Therapy Center) and S. Magness (UNC Department of Medicine) for providing lentiviral backbones.

Funding: This work was supported by the UNC Lineberger Comprehensive Cancer Center's University Cancer Research Fund, the UNC Translational and Clinical Sciences Institute, and the Eshelman Institute for Innovation (KL2TR001109, UL1TR001111, and RX03512417).

REFERENCES AND NOTES

1. Adamson C, Kanu OO, Mehta AI, Di C, Lin N, Mattox AK, Bigner DD, Glioblastoma multiforme: A review of where we have been and where we are going. Expert Opin. Investig. Drugs 18, 1061–1083 (2009).
2. Ahmed AU, Alexiades NG, Lesniak MS, The use of neural stem cells in cancer gene therapy: Predicting the path to the clinic. Curr. Opin. Mol. Ther 12, 546–552 (2010). [PubMed: 20886386]
3. Hingtgen SD, Kasmieh R, van de Water J, Weissleder R, Shah K, A novel molecule integrating therapeutic and diagnostic activities reveals multiple aspects of stem cell-based therapy. Stem Cells 28, 832–841 (2010). [PubMed: 20127797]
4. Shah K, Hingtgen S, Kasmieh R, Luiz Figueiredo J, Garcia-Garcia E, Martinez-Serrano A, Breakefield X, Weissleder R, Bimodal viral vectors and in vivo imaging reveal the fate of human neural stem cells in experimental glioma model. J. Neurosci 28, 4406–4413 (2008). [PubMed: 18434519]
5. Aboody KS, Brown A, Rainov NG, Bower KA, Liu S, Yang W, Small JE, Herrlinger U, Ourednik V, Black PML, Breakefield XO, Snyder EY, Neural stem cells display extensive tropism for pathology in adult brain: Evidence from intracranial gliomas. Proc. Natl. Acad. Sci. U.S.A 97, 12846–12851 (2000). [PubMed: 11070094]
6. Ahmed AU, Tyler MA, Thaci B, Alexiades NG, Han Y, Ulasov IV, Lesniak MS, A comparative study of neural and mesenchymal stem cell-based carriers for oncolytic adenovirus in a model of malignant glioma. Mol. Pharm 8, 1559–1572 (2011). [PubMed: 21718006]
7. Hingtgen S, Kasmieh R, Elbayly E, Nesterenko I, Figueiredo J-L, Dash R, Sarkar D, Hall D, Kozakov D, Vajda S, Fisher PB, Shah K, A first-generation multi-functional cytokine for simultaneous optical tracking and tumor therapy. PLOS ONE 7, e40234 (2012). [PubMed: 22808125]
8. Hingtgen S, Ren X, Terwilliger E, Classon M, Weissleder R, Shah K, Targeting multiple pathways in gliomas with stem cell and viral delivered S-TRAIL and Temozolomide. Mol. Cancer Ther 7, 3575–3585 (2008). [PubMed: 19001440]
9. Aboody KS, Najbauer J, Metz MZ, D'Apuzzo M, Gutova M, Annala AJ, Synold TW, Couture LA, Blanchard S, Moats RA, Garcia E, Aramburo S, Valenzuela VV, Frank RT, Barish ME, Brown CE, Kim SU, Badie B, Portnow J, Neural stem cell–mediated enzyme/prodrug therapy for glioma: Preclinical studies. Sci. Transl. Med 5, 184ra159 (2013).

10. Tobias AL, Thaci B, Auffinger B, Rincón E, Balyasnikova IV, Kwon Kim C, Han Y, Zhang L, Aboody KS, Ahmed AU, Lesniak MS, The timing of neural stem cell-based virotherapy is critical for optimal therapeutic efficacy when applied with radiation and chemotherapy for the treatment of glioblastoma. Stem Cells Transl. Med 2, 655–666 (2013). [PubMed: 23926209]
11. Aboody K, Capela A, Niazi N, Stern JH, Temple S, Translating stem cell studies to the clinic for CNS repair: Current state of the art and the need for a Rosetta stone. Neuron 70, 597–613 (2011). [PubMed: 21609819]
12. Robinton DA, Daley GQ, The promise of induced pluripotent stem cells in research and therapy. Nature 481, 295–305 (2012). [PubMed: 22258608]
13. Lujan E, Wernig M, The many roads to Rome: Induction of neural precursor cells from fibroblasts. Curr. Opin. Genet. Dev 22, 517–522 (2012). [PubMed: 22868177]
14. Lujan E, Chanda S, Ahlenius H, Südhof TC, Wernig M, Direct conversion of mouse fibroblasts to self-renewing, tripotent neural precursor cells. Proc. Natl. Acad. Sci. U.S.A 109, 2527–2532 (2012). [PubMed: 22308465]
15. Thier M, Wörsdörfer P, Lakes YB, Gorris R, Herms S, Opitz T, Seiferling D, Quandel T, Hoffmann P, Nöthen MM, Brüstle O, Edenhofer F, Direct conversion of fibroblasts into stably expandable neural stem cells. Cell Stem Cell 10, 473–479 (2012). [PubMed: 22445518]
16. Kim J, Efe JA, Zhu S, Talantova M, Yuan X, Wang S, Lipton SA, Zhang K, Ding S, Direct reprogramming of mouse fibroblasts to neural progenitors. Proc. Natl. Acad. Sci. U.S.A 108, 7838–7843 (2011). [PubMed: 21521790]
17. Han DW, Tapia N, Hermann A, Hemmer K, Höing S, Araúzo-Bravo MJ, Zaehres H, Wu G, Frank S, Moritz S, Greber B, Hun Yang J, Taek Lee H, Schwamborn JC, Storch A, Schöler HR, Direct reprogramming of fibroblasts into neural stem cells by defined factors. Cell Stem Cell 10, 465–472 (2012). [PubMed: 22445517]
18. Ring KL, Tong LM, Balestra ME, Javier R, Andrews-Zwilling Y, Li G, Walker D, Zhang WR, Kreitzer AC, Huang Y, Direct reprogramming of mouse and human fibroblasts into multipotent neural stem cells with a single factor. Cell Stem Cell 11, 100–109 (2012). [PubMed: 22683203]
19. Matsui T, Takano M, Yoshida K, Ono S, Fujisaki C, Matsuzaki Y, Toyama Y, Nakamura M, Okano H, Akamatsu W, Neural stem cells directly differentiated from partially reprogrammed fibroblasts rapidly acquire gliogenic competency. Stem Cells 30, 1109–1119 (2012). [PubMed: 22467474]
20. Kelaini S, Cochrane A, Margariti A, Direct reprogramming of adult cells: Avoiding the pluripotent state. Stem Cells Cloning 7, 19–29 (2014). [PubMed: 24627642]
21. Zhang M, Lin Y-H, Sun YJ, Zhu S, Zheng J, Liu K, Cao N, Li K, Huang Y, Ding S, Pharmacological reprogramming of fibroblasts into neural stem cells by signaling-directed transcriptional activation. Cell Stem Cell 18, 653–667 (2016). [PubMed: 27133794]
22. Carney BJ, Shah K, Migration and fate of therapeutic stem cells in different brain disease models. Neuroscience 197, 37–47 (2011). [PubMed: 21946010]
23. Young JS, Morshed RA, Kim JW, Balyasnikova IV, Ahmed AU, Lesniak MS, Advances in stem cells, induced pluripotent stem cells, and engineered cells: Delivery vehicles for anti-glioma therapy. Expert Opin. Drug Deliv 11, 1733–1746 (2014). [PubMed: 25005767]
24. Zhao D, Najbauer J, Garcia E, Metz MZ, Gutova M, Glackin CA, Kim SU, Aboody KS, Neural stem cell tropism to glioma: Critical role of tumor hypoxia. Mol. Cancer Res 6, 1819–1829 (2008). [PubMed: 19074827]
25. Sasportas LS, Kasmieh R, Wakimoto H, Hingtgen S, van de Water JA, Mohapatra G, Figueiredo JL, Martuza RL, Weissleder R, Shah K, Assessment of therapeutic efficacy and fate of engineered human mesenchymal stem cells for cancer therapy. Proc. Natl. Acad. Sci. U.S.A 106, 4822–4827 (2009). [PubMed: 19264968]
26. Kauer TM, Figueiredo J-L, Hingtgen S, Shah K, Encapsulated therapeutic stem cells implanted in the tumor resection cavity induce cell death in gliomas. Nat. Neurosci 15, 197–204 (2012).
27. Hingtgen S, Jose-Luiz F, Farrar C, Matthias D, Martinez-Quintanilla J, Bhere D, Shah K, Real-time multi-modality imaging of glioblastoma tumor resection and recurrence. J. Neurooncol 111, 153–161 (2013). [PubMed: 23242736]

28. Yamazoe T, Koizumi S, Yamasaki T, Amano S, Tokuyama T, Namba H, Potent tumor tropism of induced pluripotent stem cells and induced pluripotent stem cell-derived neural stem cells in the mouse intracerebral glioma model. Int. J. Oncol 46, 147–152 (2015). [PubMed: 25310640]

29. Yang J, Lam DH, Goh SS, Lee EX, Zhao Y, Tay FC, Chen C, Du S, Balasundaram G, Shahbazi M, Tham CK, Ng WH, Toh HC, Wang S, Tumor tropism of intravenously injected human-induced pluripotent stem cell-derived neural stem cells and their gene therapy application in a metastatic breast cancer model. Stem Cells 30, 1021–1029 (2012). [PubMed: 22311724]

30. Zhu D, Lam DH, Purwanti YI, Goh SL, Wu C, Zeng J, Fan W, Wang S, Systemic delivery of fusogenic membrane glycoprotein-expressing neural stem cells to selectively kill tumor cells. Mol. Ther 21, 1621–1630 (2013). [PubMed: 23752308]

31. Stupp R, Hegi ME, Mason WP, van den Bent MJ, Taphoorn MJB, Janzer RC, Ludwin SK, Allgeier A, Fisher B, Belanger K, Hau P, Brandes AA, Gijtenbeek J, Marosi C, Vecht CJ, Mokhtari K, Wesseling P, Villa S, Eisenhauer E, Gorlia T, Weller M, Lacombe D, Cairncross JG, Mirimanoff R-O; European Organisation for Research and Treatment of Cancer Brain Tumour, Radiation Oncology Groups, National Cancer Institute of Canada Clinical Trials Group, Effects of radiotherapy with concomitant and adjuvant temozolomide versus radiotherapy alone on survival in glioblastoma in a randomised phase III study: 5-year analysis of the EORTC-NCIC trial. Lancet Oncol 10, 459–466 (2009). [PubMed: 19269895]

32. Flax JD, Aurora S, Yang C, Simonin C, Wills AM, Billinghurst LL, Jendoubi M, Sidman RL, Wolfe JH, Kim SU, Snyder EY, Engraftable human neural stem cells respond to developmental cues, replace neurons, and express foreign genes. Nat. Biotechnol 16, 1033–1039 (1998). [PubMed: 9831031]

33. Ahmed AU, Thaci B, Tobias AL, Auffinger B, Zhang L, Cheng Y, Kwon Kim C, Yunis C, Han Y, Alexiades NG, Fan X, Aboody KS, Lesniak MS, A preclinical evaluation of neural stem cell–based cell carrier for targeted antiglioma oncolytic virotherapy. J. Natl. Cancer Inst 105, 968–977 (2013). [PubMed: 23821758]

34. Aboody KS, Najbauer J, Danks MK, Stem and progenitor cell-mediated tumor selective gene therapy. Gene Ther 15, 739–752 (2008). [PubMed: 18369324]

35. Shah K, Bureau E, Kim D-E, Yang K, Tang Y, Weissleder R, Breakefield XO, Glioma therapy and real-time imaging of neural precursor cell migration and tumor regression. Ann. Neurol 57, 34–41 (2005). [PubMed: 15622535]

36. Balyasnikova IV, Ferguson SD, Han Y, Liu F, Lesniak MS, Therapeutic effect of neural stem cells expressing TRAIL and bortezomib in mice with glioma xenografts. Cancer Lett 310, 148–159 (2011). [PubMed: 21802840]

37. Moolten FL, Wells JM, Curability of tumors bearing herpes thymidine kinase genes transferred by retroviral vectors. J. Natl. Cancer Inst 82, 297–300 (1990). [PubMed: 2299679]

38. Stupp R, Mason WP, van den Bent MJ, Weller M, Fisher B, Taphoorn MJ, Belanger K, Brandes AA, Marosi C, Bogdahn U, Curschmann J, Janzer RC, Ludwin SK, Gorlia T, Allgeier A, Lacombe D, Cairncross JG, Eisenhauer E, Mirimanoff RO; European Organisation for Research and Treatment of Cancer Brain Tumor and Radiotherapy Groups, National Cancer Institute of Canada Clinical Trials Group, Radiotherapy plus concomitant and adjuvant temozolomide for glioblastoma. N. Engl. J. Med 352, 987–996 (2005). [PubMed: 15758009]

39. Clarke RH, Moosa S, Anzivino M, Wang Y, Floyd DH, Purow BW, Lee KS, Sustained radiosensitization of hypoxic glioma cells after oxygen pretreatment in an animal model of glioblastoma and in vitro models of tumor hypoxia. PLOS ONE 9, e111199 (2014). [PubMed: 25350400]

40. McNeill RS, Vitucci M, Wu J, Miller CR, Contemporary murine models in preclinical astrocytoma drug development. Neuro Oncol 17, 12–28 (2015). [PubMed: 25246428]

41. Hirst TC, Vesterinen HM, Sena ES, Egan KJ, Macleod MR, Whittle IR, Systematic review and meta-analysis of temozolomide in animal models of glioma: Was clinical efficacy predicted? Br. J. Cancer 108, 64–71 (2013). [PubMed: 23321511]

42. Wakimoto H, Kesari S, Farrell CJ, Curry WT Jr., Zaupa C, Aghi M, Kuroda T, Stemmer-Rachamimov A, Shah K, Liu TC, Jeyaretna DS, Debasitis J, Pruszak J, Martuza RL, Rabkin SD, Human glioblastoma-derived cancer stem cells: Establishment of invasive glioma models and

treatment with oncolytic herpes simplex virus vectors. Cancer Res 69, 3472–3481 (2009). [PubMed: 19351838]

43. Morizane A, Doi D, Kikuchi T, Okita K, Hotta A, Kawasaki T, Hayashi T, Onoe H, Shiina T, Yamanaka S, Takahashi J, Direct comparison of autologous and allogeneic transplantation of iPSC-derived neural cells in the brain of a non-human primate. Stem Cell Reports 1, 283–292 (2013). [PubMed: 24319664]
44. Bagci-Onder T, Du W, Figueiredo JL, Martinez-Quintanilla J, Shah K, Targeting breast to brain metastatic tumours with death receptor ligand expressing therapeutic stem cells. Brain 138, 1710–1721 (2015). [PubMed: 25910782]
45. Nesterenko I, Wanningen S, Bagci-Onder T, Anderegg M, Shah K, Evaluating the effect of therapeutic stem cells on TRAIL resistant and sensitive medulloblastomas. PLOS ONE 7, e49219 (2012). [PubMed: 23145127]
46. Gutova M, Shackleford GM, Khankaldyyan V, Herrmann KA, Shi X-H, Mittelholtz K, Abramyants Y, Blanchard MS, Kim SU, Annala AJ, Najbauer J, Synold TW, D'Apuzzo M, Barish ME, Moats RA, Aboody KS, Neural stem cell-mediated CE/CPT-11 enzyme/prodrug therapy in transgenic mouse model of intracerebellar medulloblastoma. Gene Ther. 20, 143–150 (2013). [PubMed: 22402322]
47. Sims TL Jr., Blair Hamner J, Bush RA, Fischer PE, Kim SU, Aboody KS, McCarville B, Danks MK, Davidoff AM, Neural progenitor cell–mediated delivery of osteoprotegerin limits disease progression in a preclinical model of neuroblastoma bone metastasis. J. Pediatr. Surg 44, 204–210 (2009). [PubMed: 19159744]
48. Sena-Esteves M, Tebbets JC, Steffens S, Crombleholme T, Flake AW, Optimized large-scale production of high titer lentivirus vector pseudotypes. J. Virol. Methods 122, 131–139 (2004). [PubMed: 15542136]
49. Lassmann T, Hayashizaki Y, Daub CO, TagDust—A program to eliminate artifacts from next generation sequencing data. Bioinformatics 25, 2839–2840 (2009). [PubMed: 19737799]
50. Wu TD, Nacu S, Fast and SNP-tolerant detection of complex variants and splicing in short reads. Bioinformatics 26, 873–881 (2010). [PubMed: 20147302]
51. Wang K, Singh D, Zeng Z, Coleman SJ, Huang Y, Savich GL, He X, Mieczkowski P, Grimm SA, Perou CM, MacLeod JN, Chiang DY, Prins JF, Liu J, MapSplice: Accurate mapping of RNA-seq reads for splice junction discovery. Nucleic Acids Res 38, e178 (2010). [PubMed: 20802226]
52. Li B, Dewey CN, RSEM: Accurate transcript quantification from RNA-Seq data with or without a reference genome. BMC Bioinformatics 12, 323 (2011). [PubMed: 21816040]
53. Bullard JH, Purdom E, Hansen KD, Dudoit S, Evaluation of statistical methods for normalization and differential expression in mRNA-Seq experiments. BMC Bioinformatics 11, 94 (2010). [PubMed: 20167110]
54. Love MI, Huber W, Anders S, Moderated estimation of fold change and dispersion for RNA-seq data with DESeq2. Genome Biol 15, 550 (2014). [PubMed: 25516281]
55. Bagó JR, Pegna GJ, Okolie O, Hingtgen SD, Fibrin matrices enhance the transplant and efficacy of cytotoxic stem cell therapy for post-surgical cancer. Biomaterials 84, 42–53 (2016). [PubMed: 26803410]
56. Bagó JR, Pegna GJ, Okolie O, Mohiti-Asli M, Loboa EG, Hingtgen SD, Electrospun nanofibrous scaffolds increase the efficacy of stem cell-mediated therapy of surgically resected glioblastoma. Biomaterials 90, 116–125 (2016). [PubMed: 27016620]
57. Wynn RF, Hart CA, Corradi-Perini C, O'Neill L, Evans CA, Wraith JE, Fairbairn LJ, Bellantuono I, A small proportion of mesenchymal stem cells strongly expresses functionally active CXCR4 receptor capable of promoting migration to bone marrow. Blood 104, 2643–2645 (2004). [PubMed: 15251986]

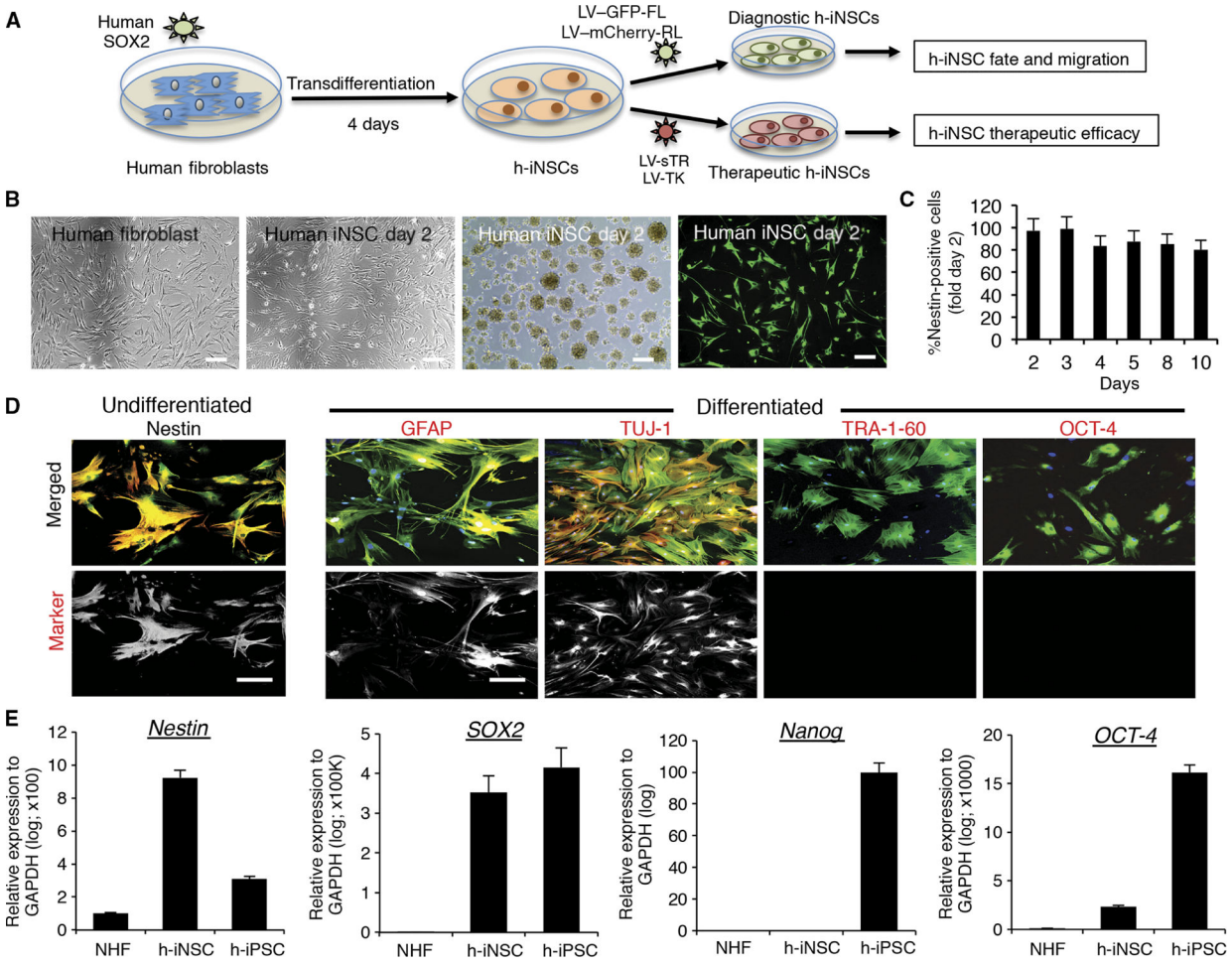

Fig. 1. Generation and characterization of diagnostic and therapeutic h-iNSC^{TE}.

(A) Schematic depiction of the strategy used to create therapeutic and diagnostic variants of h-iNSC^{TE}. Human fibroblasts were transduced with SOX2 and placed in NSC-inducing medium. After 4 days, the h-iNSC^{TE} were expanded and transduced with optical reporters or tumoricidal transgenes. (**B**) White light and fluorescence photomicrographs of human fibroblasts and h-iNSC^{TE} grown as monolayers and neurospheres or stained with antibodies against nestin (green). (**C**) Summary graph showing the expression of nestin over time at different days after induction of h-iNSC^{TE} generation. (**D**) Immunofluorescence staining showing h-iNSC^{TE}–GFP (green) expression of the NSC marker nestin (red) and GFAP^{+} astrocytes and TUJ-1^{+} neurons after differentiation by mitogen removal (staining shown in red). In contrast, no staining was observed for the pluripotency markers TRA-1–60 or OCT-4. Hoechst staining is shown in blue. Fluorescence images showing only the red (555 nm) secondary antibody channel are shown in the bottom row. (**E**) RT-PCR analysis of nestin, SOX2, nanog, and OCT-4 expression in NHF, h-iNSC^{TE}, and h-iPSCs. Data in (C) and (E) are shown as means ± SEM (error bars are from three to four independent experiments; $n = 3$ technical replicates). Scale bars, 200 μm. GAPDH, glyceraldehyde-3-phosphate dehydrogenase.

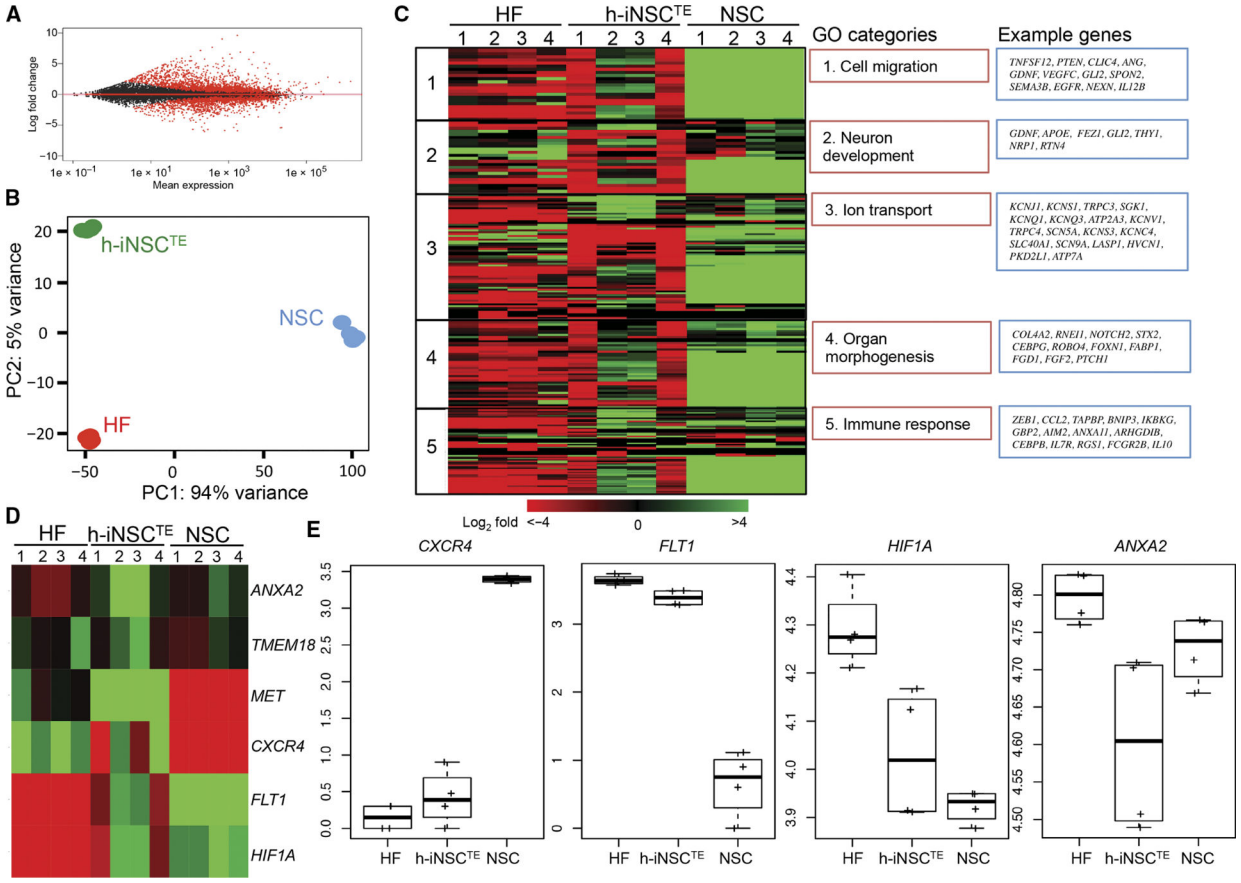

Fig. 2. Transcriptome changes as fibroblasts are converted into h-iNSC^{TE}.

Differential expression analysis (**A**) and principal components analysis (PCA) (**B**) revealed differences in gene expression between parental human fibroblasts (HF) and h-iNSC^{TE}. (**C**) Ontology analysis showing the differential gene expression between human fibroblasts, h-iNSC^{TE}, and brain-derived NSCs. Biological replicates are indicated by the numbers above each column. Gene ontology (GO) and example genes are shown in the red and blue boxes, respectively. (**D**) Heat map revealing the expression of six different tumor-homing migration genes across human fibroblasts, h-iNSC^{TE}, and NSCs. Down- and up-regulated genes are indicated by red and green, respectively. (**E**) Box plots showing relative expression of tumor-homing genes *CXCR4*, *FLT1*, *HIF1A*, and *ANXA2*. The box represents the 25th and 75th percentile, and the whiskers represent 1.5 × interquartile range (n = 3 technical replicates).

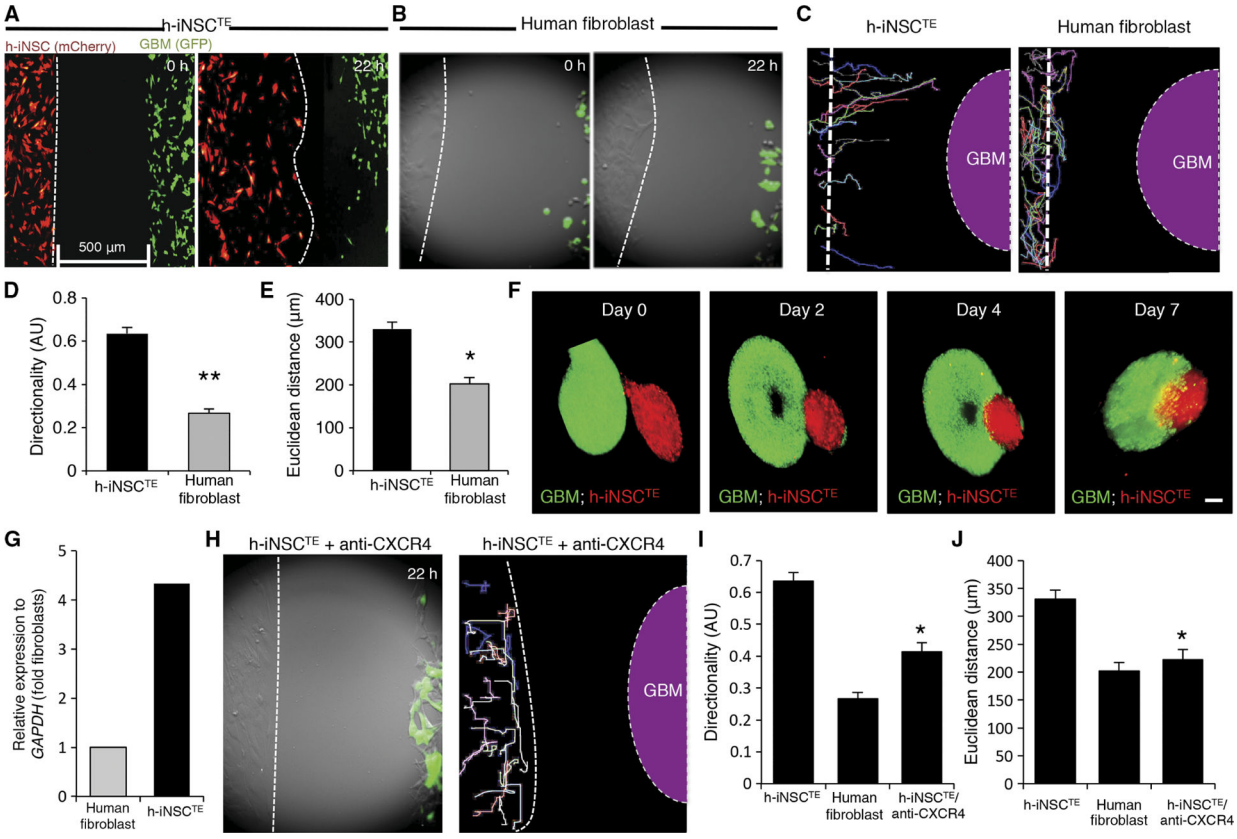

Fig. 3. Engineered h-iNSC^{TE} homing to GBM.

h-iNSC^{TE}–mC-FL were seeded 500 μm away from mCherry-expressing human GBM cells and placed in a fluorescence incubator microscope. Time-lapse fluorescence images were captured every 20 min for 22 hours and used to construct movies that revealed the migration of h-iNSC^{TE} to GBM in real time. (**A** and **B**) Summary images showing migration of h-iNSC^{TE}–mC-FL (red) (A) or parental human fibroblasts (B) toward U87–GFP-FL (green) at 0 and 22 hours after plating. (**C**) Single-cell tracings depicting the paths of h-iNSC^{TE}–mC-FL or human fibroblast–directed migration toward GBM over 22 hours. Dashed line indicates the site of GBM seeding. (**D** and **E**) Summary graphs showing the directionality (D) and Euclidean distance (E) of h-iNSC^{TE} or fibroblast migration toward GBM cells determined from the real-time motion analysis. $^{**}P = 0.00001$, $^{*}P = 0.00049$ by Student's *t* test. (**F**) Fluorescence imaging showed the migration of h-iNSC^{TE}–mC-FL (red) into U87 spheroids (green) and their penetration toward the core of the tumor spheroid over time in 3D levitation culture systems. (**G**) Summary graph of RT-PCR analysis showing the increased expression of *CXCR4* in h-iNSC^{TE} compared to fibroblasts. (**H**) Summary image and cell tracings showing the attenuated migration of h-iNSC^{TE} after pretreatment with CXCR4-blocking antibody. (**I** and **J**) Summary graphs demonstrating a reduction in directional migration (I) ($^{*}P = 0.0000013$ by Student's t test) and Euclidean distance (J) ($^{*}P = 0.0000247$ by Student's *t* test) by h-iNSC^{TE} treated with anti-CXCR4 antibodies. Data in (D), (E), (I), and (J) are means ± SEM of three independent experiments performed in triplicate. Scale bars, 200 μm.

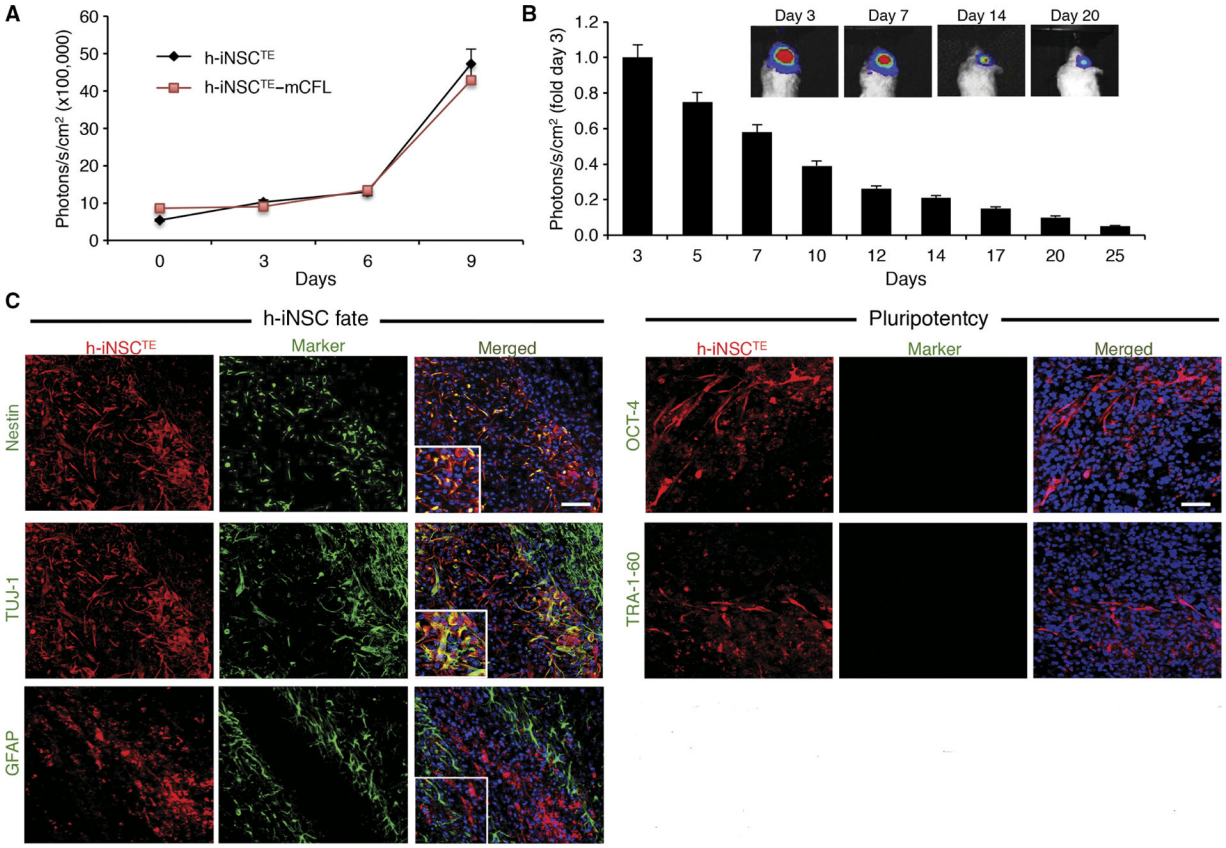

Fig. 4. In vivo characterization of h-iNSC^{TE} transplanted into the mouse brain.

(**A**) Summary graph demonstrating the proliferation of unmodified h-iNSC^{TE} and h-iNSC^{TE} engineered to express mCherry/FL. No significant difference was found by two-way analysis of variance (ANOVA). (**B** and **C**) h-iNSC^{TE}–mC-FL were implanted into the frontal lobes of mice, and serial BLI was used to monitor their persistence over 3 weeks. Summary graphs demonstrated that the h-iNSC^{TE} persisted for 25 days, although they were gradually cleared (B). Immunofluorescence analysis of h-iNSCTE (red) 14 days after implantation into the brain showed nestin^{+} and TUJ-1^{+} cells, but minimal h-iNSCTE stained positive for the astrocyte maker GFAP or the pluripotency markers OCT-4 and TRA-1–60 (green) (C). Data in (A) and (B) are means ± SEM. (A) and (B) represent three different experiments performed in triplicate. Scale bars, 50 μm (C).

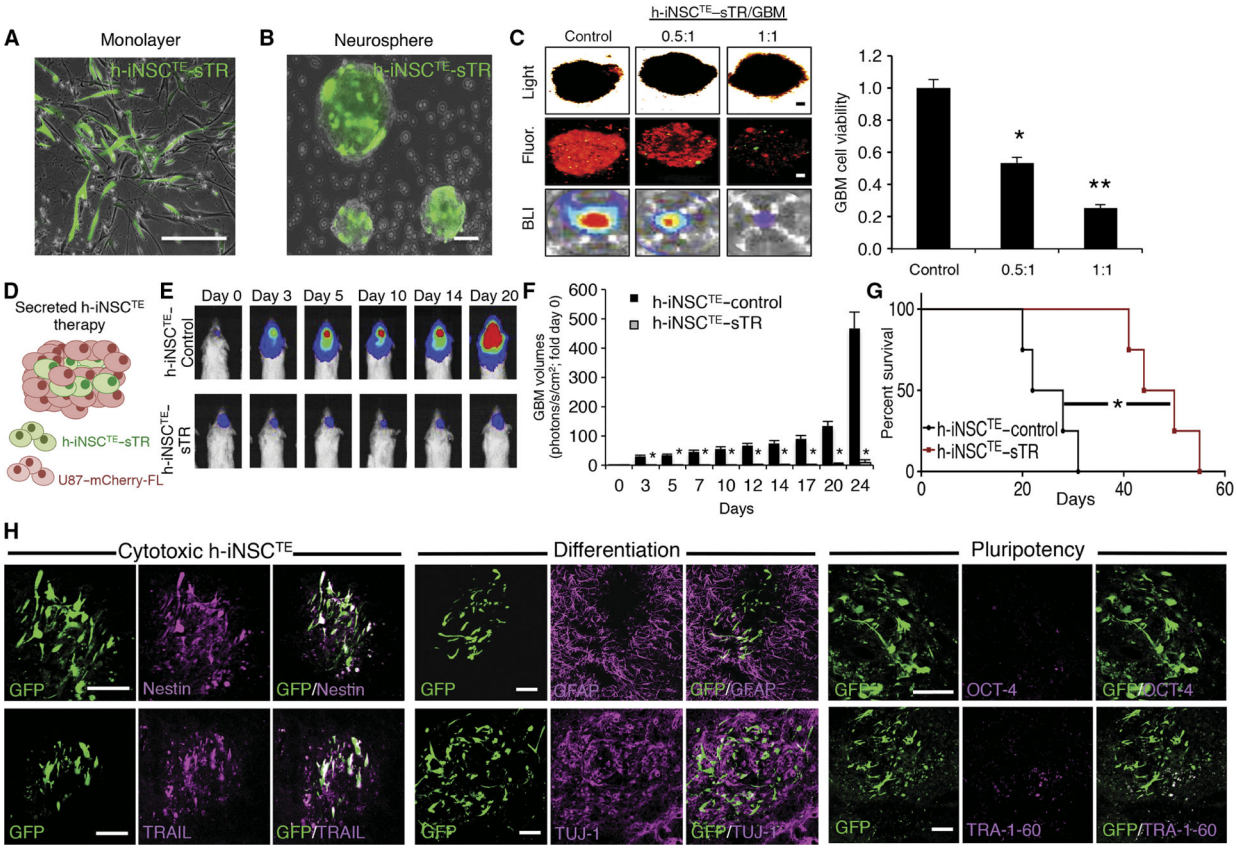

Fig. 5. h-iNSC^{TE}–mediated TRAIL therapy for solid GBM.

(**A** and **B**) Representative fluorescence photomicrographs depict h-iNSC^{TE} engineered to secrete the proapoptotic agent TRAIL and grown in a monolayer (A) or as floating neurospheres (B). Expression of the internal ribosomal entry sites (IRES)–GFP element present in the construct is shown in green. (**C**) Images and summary data of 3D suspension cultures showing the viability of mCherry^{+} human U87 GBM spheroids (red) mixed with therapeutic h-iNSC^{TE}–sTR or control cells at a ratio of 0.5:1 or 1:1. GBM spheroid viability was determined by BLI 48 hours after treatment. $^{**}P = 0.0169$, $^{*}P = 0.038$ by ANOVA. (**D**) h-iNSC^{TE}–sTR therapy for solid GBM was performed by xenografting a mixture of h-iNSC^{TE}–sTR and U87 GBM cells into the brain parenchyma of severe combined immunodeficient mice. (**E** and **F**) Representative BLI (E) and summary data (F) demonstrating the inhibition of solid U87 GBM progression by h-iNSC^{TE}–sTR therapy compared to control-treated mice. $^{*}P = 0.0044$ by repeated-measures ANOVA. **(G)** Kaplan-Meier survival curves demonstrating the extension in survival in h-iNSC^{TE}–sTR–treated animals compared to h-iNSC^{TE}–control. $^{*}P = 0.0067$ by log-rank test. (**H**) Representative images demonstrating the expression of cytotoxic, differentiation, and pluripotency markers in h-iNSC^{TE}–sTR after therapy. A subset of animals were sacrificed 14 days after therapy; brain sections were stained with antibodies against nestin, TRAIL, GFAP, TUJ-1, OCT-4, or TRA-1–60; and the colocalization between staining (magenta) and GFP^{+} h-iNSC^{TE}–sTR (green) was visualized. Data in (C) are means ± SEM of three independent experiments performed in triplicate. Data in (F) are means ± SEM. Scale bars, 100 μm.

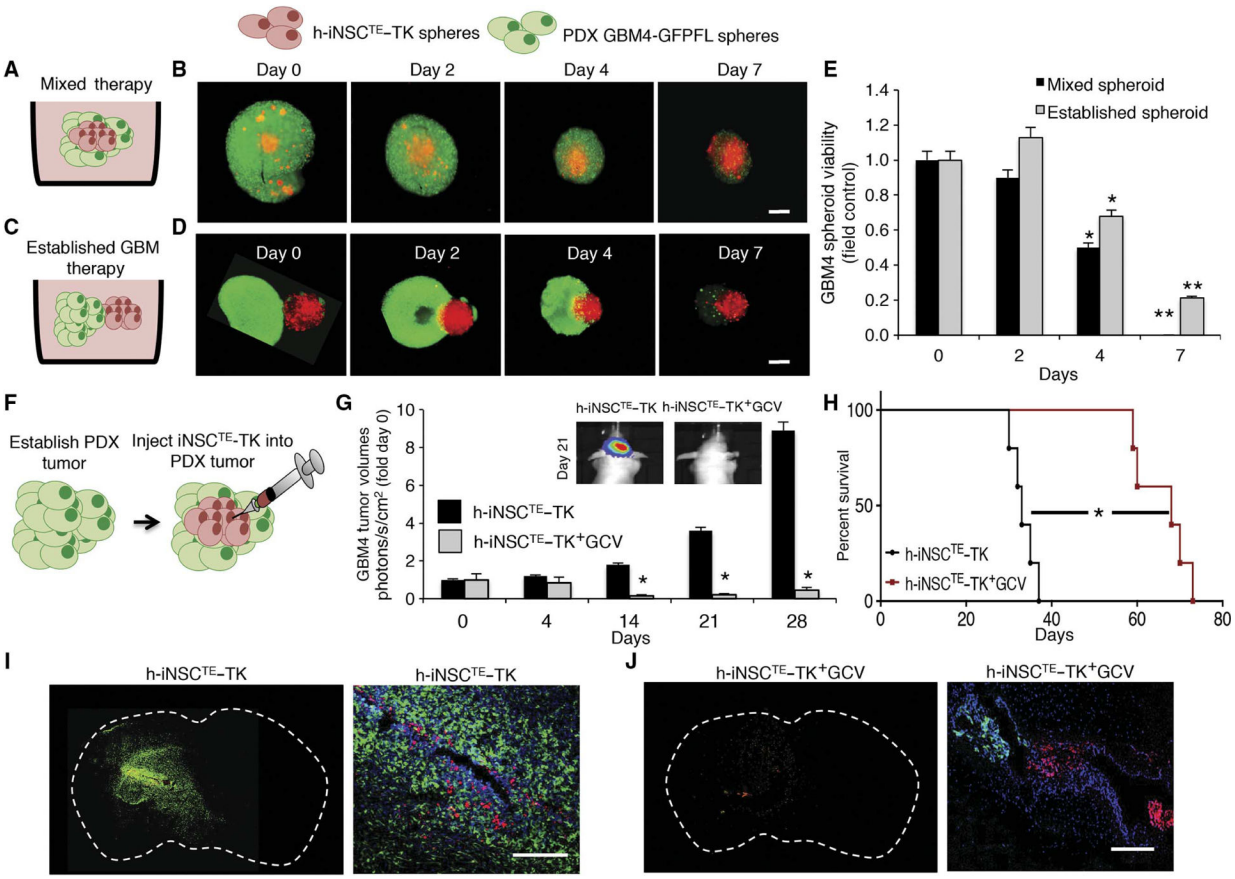

Fig. 6. h-iNSC^{TE} prodrug/enzyme therapy for human patient–derived GBMs.

(A to **D)** The antitumor effects of h-iNSC^{TE}–TK therapy were determined in two different 3D culture models. h-iNSC^{TE}–TK (red) were either mixed GFP^{+} GBM4 patient-derived GBM cells (A and B) or seeded adjacent to established GBM4 spheroids (C and D), and GCV was added to initiate tumor killing. Serial fluorescence images showed the time-dependent decrease in GBM4 spheroid volume by h-iNSC^{TE}–TK^{+}GCV therapy. (**E**) Summary graph demonstrating the reduction in GBM4 spheroid volume over 7 days by h-iNSC^{TE}–TK^{+}GCV therapy either mixed or seeded adjacent to established spheroids. $^{**}P = 0.0099$, $^{*}P = 0.048$ by ANOVA. (**F** to **H**) h-iNSC^{TE}–TK therapy was assessed in vivo by injecting h-iNSC^{TE}–TK cells into GBM4 tumors established 10 days earlier in the brains of mice (F). Serial BLI showed that the progression of GBM4 tumors was inhibited by h-iNSC^{TE}–TK^{+}GCV therapy (G). $^{*}P = 0.0046$ by repeated-measures ANOVA. (H) Kaplan-Meier survival curves demonstrate the survival of mice bearing GBM4 tumors treated with h-iNSC^{TE}–TK^{+}GCV therapy or control h-iNSC^{TE}. $^{*}P = 0.0018$ by log-rank test. (**I** and **J**) Representative whole-brain and high-magnification images showing cell nuclei (blue), GBM4 (green), and h-iNSC^{TE}–TK (red) distribution 21 days after delivering h-iNSC^{TE}–control (I) or h-iNSC^{TE}–TK (J) into established GBM4 tumors. A large GBM4 tumor was present in the control h-iNSC^{TE}–TK animals, and only a small GBM4 focus was detected in mice treated with h-iNSC^{TE}–TK^{+}GCV. Data in (E) are means ± SEM of three independent experiments performed in triplicate. Data in (G) are means ± SEM. Scale bars, 400 mm (B and D) and 200 μm (I and J).

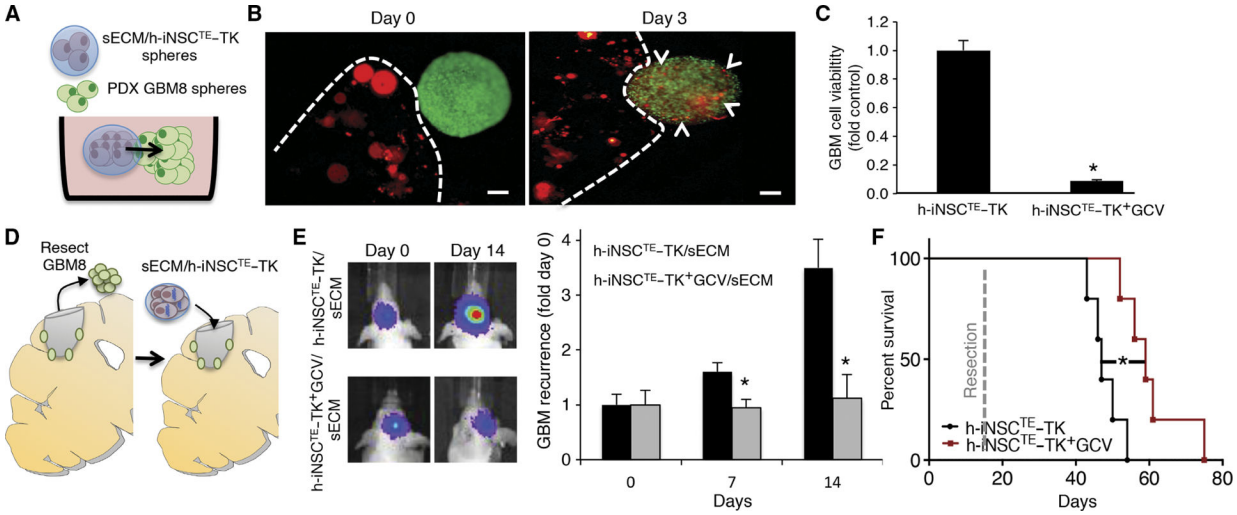

Fig. 7. Intracavity h-iNSC^{TE}–TK therapy for surgically resected diffuse GBMs.

(**A** to **C**) 3D suspension cultures were used to assess the migration and antitumor efficacy of sECM-encapsulated h-iNSC^{TE}–TK against patient-derived GBM8 spheroids (A). h-iNSC^{TE}–TK (red) encapsulated in sECM were found to migrate from the matrix and populate GBM8 spheroids 3 days after seeding (B). Summary data demonstrate that h-iNSC^{TE}–TK (red) encapsulated in sECM reduce the volume of GBM8 spheroids (green) after GCV treatment compared to spheroids treated without GCV (C). *P = 0.0016 by Student's t test. (**D** to **F**) To mimic clinical h-iNSC^{TE} therapy for surgically resected GBM, h-iNSC^{TE}–TK were encapsulated in sECM and transplanted into the surgical cavity after resection of diffuse patient-derived GBM8 tumors expressing GFP-FL (D). Representative images and summary data for serial imaging demonstrating the inhibition of tumor recurrence after intracavity h-iNSC^{TE}–TK therapy for postoperative minimal GBM8 tumors (E). *P = 0.0072 by repeated-measures ANOVA. Kaplan-Meier survival curves of mice that underwent surgical resection of diffuse patient-derived GBM8 tumor cells and were treated with control h-iNSC^{TE} or h-iNSC^{TE}–TK encapsulated in sECM and transplanted into the surgical cavity (F). *P = 0.0064 by log-rank test. Data in (C) are means ± SEM of three independent experiments performed in triplicate. Data in (E) are means ± SEM. Scale bars, 200 μm.